Experimental Measurement of the Divergent Quantum Metric of an Exceptional Point

Qing Liao,[1,*] Charly Leblanc,[2] Jiahuan Ren,[1,3] Feng Li,[4,†] Yiming Li,[4] Dmitry Solnyshkov,[2,5,‡] Guillaume Malpuech,[2] Jiannian Yao,[3] and Hongbing Fu[1,3]

[1]*Beijing Key Laboratory for Optical Materials and Photonic Devices, Department of Chemistry, Capital Normal University, Beijing 100048, People's Republic of China*

[2]*Institut Pascal, PHOTON-N2, Université Clermont Auvergne, CNRS, SIGMA Clermont, Institut Pascal, F-63000 Clermont-Ferrand, France*

[3]*Tianjin Key Laboratory of Molecular Optoelectronic Sciences, Department of Chemistry, School of Sciences, Tianjin University, Collaborative Innovation Center of Chemical Science and Engineering, Tianjin 300072, People's Republic of China*

[4]*Key Laboratory for Physical Electronics and Devices of the Ministry of Education, Shaanxi Key Lab of Information Photonic Technique, School of Electronic and Information Engineering, Xi'an Jiaotong University, Xi'an 710049, People's Republic of China*

[5]*Institut Universitaire de France (IUF), 75231 Paris, France*

(Received 15 December 2020; accepted 21 July 2021; published 1 September 2021)

The geometry of Hamiltonian's eigenstates is encoded in the quantum geometric tensor (QGT), containing both the Berry curvature, central to the description of topological matter, and the quantum metric. So far, the full QGT has been measured only in Hermitian systems, where the role of the quantum metric is mostly limited to corrections. On the contrary, in non-Hermitian systems, and, in particular, near exceptional points, the quantum metric is expected to diverge and to often play a dominant role, for example, in the enhanced sensing and in wave packet dynamics. In this Letter, we report the first experimental measurement of the quantum metric in a non-Hermitian system. The specific platform under study is an organic microcavity with exciton-polariton eigenstates, which demonstrate exceptional points. We measure the quantum metric's divergence, and we determine the scaling exponent $n = -1.01 \pm 0.08$, which is in agreement with the theoretical description of second-order exceptional points.

DOI: 10.1103/PhysRevLett.127.107402

The recent development of experimental techniques and theoretical understanding has allowed one to measure both components of the quantum geometric tensor (QGT) [1–3], which are the Berry curvature and the quantum metric, experimentally [4,5]. In particular, the use of optical systems allows one to access the nontrivial geometry of real photonic bands and to observe the related consequences on wave packet propagation and the anomalous Hall effect [5]. In Hermitian systems, the quantum metric determines the nonadiabatic corrections to the anomalous Hall effect [6–8], with the dominant role played by the Berry curvature. These measurements have inspired further research on the quantum metric [3], adding on top of the previous works that have demonstrated its importance for superfluidity in flat bands [9,10], the electronic magnetic susceptibility [6,11], the characterization of general phase transitions [12,13], or the exciton Lamb shift [14].

At the same time, studies of non-Hermitian systems [15–18] have also started to deal with the topology of the exceptional points, which are the branch points of the multivalued Riemann surface formed by the eigenvalues of the Hamiltonian of such systems. It was shown that the chiral dynamics associated with this non-Hermiticity is extremely promising for applications [19–21], together with the enhanced sensing properties [22]. Crucially, the good topological invariant in the vicinity of these points is not anymore associated with the Berry curvature of the eigenstates but with the winding number of the so-called effective field [23,24] (and the associated complex eigenvalues), determined by the Hermitian and non-Hermitian parts of the Hamiltonian itself. Indeed, because of the non-Hermitian contribution, the adiabatic description of dynamics based on the Berry curvature becomes irrelevant [25,26]. On the other hand, the quantum metric should exhibit a hyperbolic divergence at the exceptional points of second order (with square root topology) [27,28]. This divergence has remarkable physical consequences, controlling the dynamics of wave packets centered at exceptional points [28]. Here, the quantum metric is not responsible for small corrections; it has a dominant role, determining a nonvanishing constant group velocity with a polarization-dependent direction. However, the quantum metric of a non-Hermitian system has never been measured experimentally so far, in spite of the extended studies of such points in optics [18,29], which date back to Voigt [30], and of their recent observation in microcavities [31].

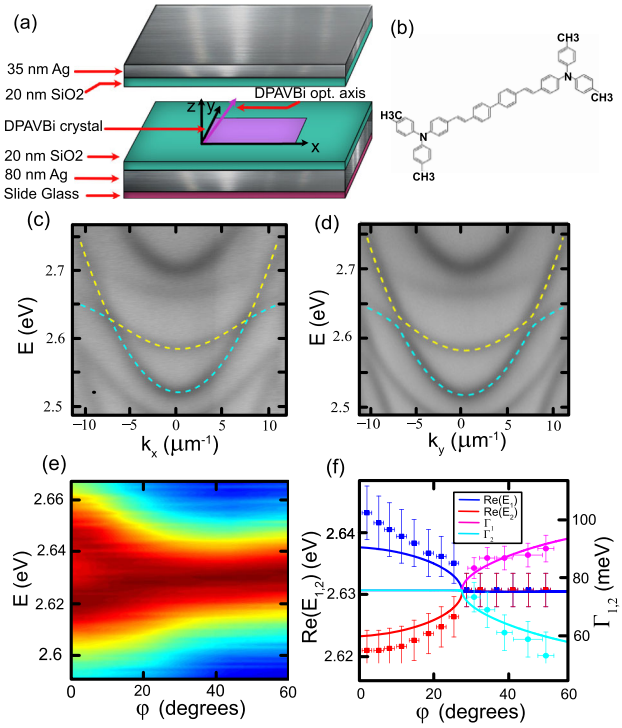

FIG. 1. Reflectivity of the organic microcavity. (a) Scheme of the microcavity sample. (b) Structure of the DPAVBi molecule. (c),(d) Reflectivity as a function of wave vector k_x and k_y (respectively) and energy, exhibiting anticrossing along k_y. (e) Reflectivity as a function of the in-plane polar angle ϕ and energy E for $|k| = |k^*|$ (EP wave vector). (f) Real and imaginary parts of the mode energies (dots with error bars, experiment; lines, theory).

In this work, we study the modes of an organic microcavity [32] exhibiting a polarization-dependent strong coupling, which provides a pronounced non-Hermitian response ensuring well-defined exceptional points (EPs). We measure the Stokes parameters of the eigenmodes in vicinity of the exceptional points and extract the corresponding quantum metric. We demonstrate that this metric is diverging, exhibiting a scaling exponent $n = -1.01 \pm 0.08$. The coefficients of the measured hyperbola correspond to the analytical predictions based on an effective Hamiltonian.

The sample we study is an organic microcavity with metallic mirrors, shown in Fig. 1(a) [33]. The active layer is a microcrystal of an organic molecule, 4,4′-bis[4-(di-*p*-tolylamino)styrylbiphenyl (DPAVBi), whose structure is shown in Fig. 1(b). The microbelt width (Y axis) is around 20 μm, with a thickness of 2.0–3.0 μm, and the length (oriented along X) is several hundreds of micrometers. The triclinic form of the DPAVBi crystal is determined by the specific arrangement of molecules. The resulting optical properties of the crystal are strongly anisotropic, with an optical axis in the XZ plane (cyan arrow) tilted by 36° [33] with respect to the Z axis.

We begin by showing the unpolarized reflectivity of the sample in the two orthogonal directions [Figs. 1(c) and 1(d)]. Angle-resolved spectroscopy was measured using a halogen lamp with a wavelength range of 400–700 nm. The light was entered and collected by using the 100× microscope objective with a high aperture (0.95); the collection angle can achieve ±70°. The momentum space of the reflectivity was located at the back focal plane of the objective lens. The reflectivity is plotted as a function of energy and wave vectors k_x and k_y. We focus on two particular eigenmodes, which exhibit the clearest behavior. First of all, we note that the two branches show very different effective masses and very different linewidths. This is due to the strongly polarized nature of excitons in DPAVBi (see [33,34] on the anisotropy of the excitonic absorption by the microbelt). The exciton ($E_X \sim 2.7$ eV) strongly couples with the photonic modes only in the H polarization (electric field aligned along X) exhibiting a Rabi splitting of 80 meV. The V-polarized modes (electric field aligned along Y) remain unaffected by the excitonic resonance. The strongly coupled modes exhibit a higher mass and a smaller linewidth, both because of their reduced photonic fraction.

In the two k-space directions, the behavior of the two modes is qualitatively different: A crossing of the weakly and strongly coupled polarization branches occurs along the k_x direction and an anticrossing along k_y. This anticrossing is *not* the result of the above-mentioned strong exciton-photon coupling. It is rather due to the emergent optical activity of the structure, which becomes sufficiently large at the anticrossing wave vector. Optical activity has recently been shown to emerge at the macroscopic level in cavity structures, when the linear birefringence is so high that oppositely polarized modes of opposite parity become degenerate [35,36]. It is therefore a coupling which occurs between the photonic part of such modes. This is illustrated in Supplemental Fig. S2 [34], showing (with a thicker sample) that the anticrossing appears only for opposite parity branches. The direction of the optical activity is determined by the tilt of the optical axis [35]: it emerges in the direction Y, perpendicular to the plane XZ containing the optical axis of the crystal.

The two closest branches can be described by a 2×2 effective non-Hermitian Hamiltonian describing two polarization subbands with two different effective masses stemming from a different coupling with the exciton. The eigenvectors of this two-band Hamiltonian are mapped to the Stokes vector of light. The non-Hermitian contribution has to be included because of the difference of the linewidths. This effective Hamiltonian written in the *linear* polarization basis reads (more details on its derivation are given in Ref. [34])

$$H_0 = \begin{pmatrix} \beta_0 + (\xi - \beta)(k_x^2 + k_y^2) - i\Gamma - i\Gamma_0 & \chi k_y \\ \chi k_y & -\beta_0 + (\xi + \beta)(k_x^2 + k_y^2) + i\Gamma - i\Gamma_0 \end{pmatrix}. \quad (1)$$

This Hamiltonian describes two linearly (H and V) polarized modes. They have different effective masses (the $\pm\beta k^2$ term): V is a purely photonic mode with a mass m_V, while H is strongly coupled with excitons and, thus, has a larger effective mass $m_H > m_V$ [34]. Because of the same reason, they also exhibit different linewidths: The strongly coupled H mode is narrower (the $\pm i\Gamma$ term). Finally, these two linearly polarized modes are coupled by the optical activity term χk_y acting only along the Y axis. β_0 represents the splitting of the two modes at $k = 0$, $\xi = \hbar^2/2m^*$ with $m^* = [2m_H m_V/(m_H + m_V)]$, χ represents the emergent optical activity, Γ is the half-difference of the broadenings of the modes, and Γ_0 is the half-average of the broadenings. Finally, β is the difference of the effective masses of the two modes, which comes from the fact that one mode is coupled with the exciton, while there is no coupling for the other mode. The theoretical dispersions calculated with the Hamiltonian (1) are shown in Figs. 1(c) and 1(d) with dashed lines. The best fit is obtained with the following parameters: $\beta_0 = 130 \pm 9$ meV, $\Gamma = 11 \pm 4$ meV, $\beta = (1.00 \pm 0.07)$ meV/μm^{-2}, $m^* = (2.0 \pm 0.1) \times 10^{-5} m_e$, and $\chi = 1.8 \pm 0.6$ meV/μm^{-1}.

The Hamiltonian is symmetric versus k_x and antisymmetric versus k_y. Since the branches are crossing along k_x and anticrossing along k_y, there are necessarily four points at which the transition between the crossing and the anticrossing occurs. These are the famous exceptional points characteristic for non-Hermitian systems. The plot of experimentally measured reflectivity spectra along a circle of constant $|k|$ passing through one of the exceptional points is shown in Fig. 1(e). The extracted mode energies and linewidths are shown in Fig. 1(f) with points, and the corresponding real and imaginary parts of the theoretical eigenenergies appear as solid lines. The extraction is performed by fitting the reflectivity spectra with Lorentzians (see [34], Fig. S4). In systems with perfectly balanced gain and losses, the exceptional points correspond to the transition between the PT-symmetric regime with real eigenvalues and the PT-broken regime with imaginary eigenvalues [37]. The same transition is still present in our case, in spite of the overall decay Γ_0, and the observed behavior of the modes confirms the presence of a second-order exceptional point at k^*.

The eigenvalues do not tell everything about physical systems: The corresponding eigenstates are also important. While the famous Berry curvature and its integral, the Chern number, seem to be less relevant for non-Hermitian systems in the vicinity of exceptional points due to the essentially nonadiabatic behavior [25,26], other quantities linked with the eigenstates, such as the quantum metric, play a key role in the wave packet (beam) dynamics [28]. The measurement of the Stokes vector for each eigenstate in reciprocal space [5,7] allows one to extract the quantum metric using the definition of the quantum geometric tensor (whose real part is the quantum metric, and the imaginary part is the Berry curvature):

$$g_{ij} = \mathrm{Re}[\langle \nabla\psi | \nabla\psi \rangle - \langle \psi | \nabla\psi \rangle \langle \nabla\psi | \psi \rangle], \quad (2)$$

where $|\psi\rangle$ is the eigenstate written as a spinor (similar to the Jones vector, but on the circular basis) as follows:

$$|\psi\rangle = \begin{vmatrix} \cos\frac{\theta}{2} e^{-i\phi} \\ \sin\frac{\theta}{2} \end{vmatrix} \quad (3)$$

and the angles $\theta = \arccos S_3$ and $\phi = \arctan S_2/S_1$ characterize the orientation of the Stokes vector. We note that the gradient is taken in the parameter space (the reciprocal space). We now focus on a quarter of the reciprocal space containing a single exceptional point and extract the Stokes vectors of the modes from polarization-resolved reflectivity measurements. In order to investigate the polarization properties, we placed a linear polarizer, a half-wave plate, and a quarter-wave plate in front of the spectrometer slit to obtain the polarization state of each pixel in the k-space, horizontal-vertical (0° and 90°), diagonal (±45°), and circular ($\sigma+$ and $\sigma-$) basis. An energy spectrum is obtained in each of the six polarizations (H, V, D, A, L, and R) for each point of the reciprocal space. We use a Lorentzian fit in order to get the positions, the relative intensities I, and the widths of the two modes, which permits the extraction of a 2D reciprocal space map of the Stokes vector components S_1, S_2, and S_3 of the lower branch, shown in Figs. 2(a)–2(c). The validity of the effective 2×2 Hamiltonian (1) is confirmed by the good fit of the dispersions in Figs. 1(c) and 1(d) and by the agreement between the experimentally extracted components of the Stokes vector [Figs. 2(a)–2(c)] and the theoretically calculated ones [Figs. 2(d)–2(f)]. The EP located at $k_x^* = 4.01$ μm^{-1} and $k_y^* = 6.12$ μm^{-1} is shown by a white star. The two components S_1 and S_3 cancel at this point, while S_2 exhibits a maximum (similar to the circular polarization observed at the Voigt points).

Once the Stokes vectors are known, one can extract the quantum metric elements using Eq. (2), as described in detail in Ref. [7]. The results of this extraction are shown as a 2D plot of the trace of the quantum metric $g_{xx} + g_{yy}$ in Fig. 3(a). The uncertainty of the extracted points is of the

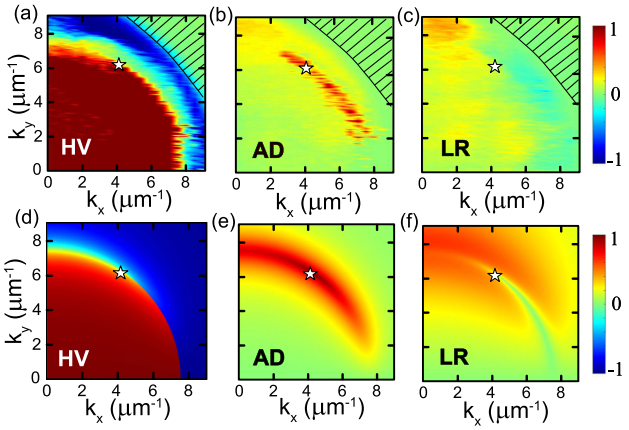

FIG. 2. Stokes vector components of the lowest-energy eigenstates (experiment and theory). (a)–(c) Experiment (S_1, S_2, S_3); (d)–(f) theory (S_1, S_2, S_3). A region where the pseudospin could not be extracted experimentally is hatched.

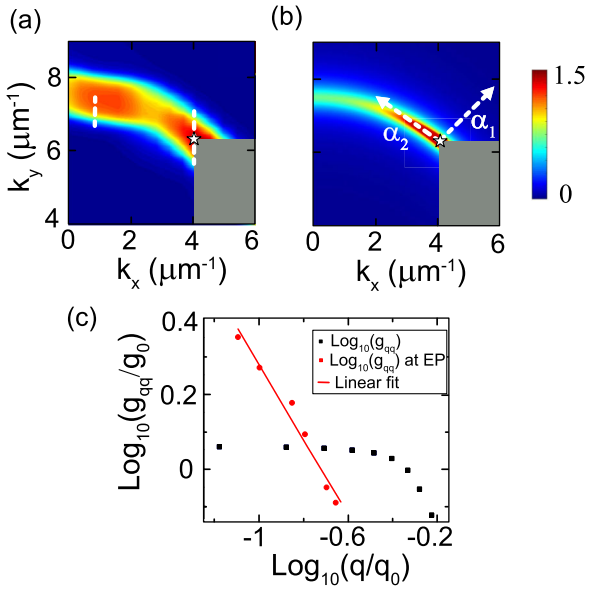

FIG. 3. Quantum metric of an exceptional point. 2D maps of the trace of the quantum metric in the vicinity of an EP marked as a star: (a) experiment; (b) theory. The gray region covers the discontinuity of the wave function (branch cut). (c) A log-log plot of the experimentally extracted quantum metric g_{qq} near $k_x = 0$ (black dots) and near the EP (red dots) and its fit (red line), giving the scaling exponent $n = -1.01 \pm 0.08$. The metric is extracted along the white dashed lines shown in (a).

order of 10% [5]. The part of the reciprocal space corresponding to the branch cut of the Riemann surface formed by the eigenstates is covered by a gray rectangle. The rectangular shape of the remaining regions facilitates their numerical treatment. A clear maximum is visible in the vicinity of the EP. The global behavior of the metric is in a good agreement with theoretical predictions based on the eigenstates of the Hamiltonian (1) [Fig. 3(b)].

The quantum metric is known to diverge hyperbolically at the exceptional points of the second order (with two crossing branches) [27,28], and an explicit expression for the metric in the vicinity of the exceptional point can be written as

$$g_{qq} = \frac{\sqrt{\alpha_1^2\cos^2\phi' + \alpha_2^2\sin^2\phi'}}{8\Gamma q} + \frac{\alpha_1^2\cos^2\phi' + \alpha_2^2\sin^2\phi'}{16\Gamma^2} \tag{4}$$

where q is the wave vector measured from the exceptional point and $\alpha_{1,2}$ [orientation shown by white arrows in Fig. 3(b)] are proportional to the difference of the group velocities at the crossing point (the celerity of the effective Dirac Hamiltonian; see [34] for details). Experimentally, the values of the quantum metric are obtained only for a finite number of pixels in the reciprocal space, which can be close to the exceptional point but never fall on it exactly. In order to demonstrate the hyperbolic divergence, we choose a particular direction in the reciprocal space, where the experimental resolution is the highest (k_y), and plot in Fig. 3(c) the quantum metric in log-log scale for several experimental points (red dots) closest to the exceptional point as a function of $q = |k_y - k_y^*|$ (using $q_0 = 1\ \mu\text{m}^{-1}$ and $g_0 = 1\ \mu\text{m}^2$ as characteristic scales). A fit with a power law $g_{qq} \sim q^n$ (black line) allows one to determine the scaling of the quantum metric $n = -1.01 \pm 0.08$. The divergent behavior is best visible in comparison with another region, which exhibits a finite maximum [black points in Fig. 3(c)] appearing as a horizontal asymptotic in log-log scale. Both regions are shown in Fig. 3(a) as white lines. We can, therefore, conclude that we have observed the hyperbolic divergence of the quantum metric of a second-order exceptional point experimentally.

The agreement between the experiment and the theory can be checked further, by extracting the second (constant) term from the trace of the quantum metric and comparing it with the parameters of the effective Hamiltonian (1) obtained from the dispersions shown in Figs. 1(c) and 1(d). For this, we fit the experimentally extracted values of the quantum metric with a function $f(q)$ corresponding to the reduced expression (4) of the quantum metric tensor g_{qq}:

$$f = \frac{\eta}{q} + 4\eta^2. \tag{5}$$

The fit of the metric gives $\eta = 0.173 \pm 0.004\ \mu\text{m}$. On the other hand, $\eta \approx \sqrt{\alpha_1^2 + \alpha_2^2}/8\sqrt{2}\Gamma$. We take the parameters of the Hamiltonian extracted from the fit of the experimental dispersion in Fig. 1: $\Gamma = 11 \pm 0.4$ meV and the celerity parameter $\sqrt{\alpha_1^2 + \alpha_2^2}/\sqrt{2} = 14 \pm 2\ \text{meV}/\mu\text{m}^{-1}$, which gives $\eta_{\text{exp}} = 0.16 \pm 0.06\ \mu\text{m}$. This agreement validates both the metric extraction procedure and the theoretical analysis of the Hamiltonian and its eigenstates.

Our results demonstrate the advantages of the optical systems for the studies of advanced quantum-mechanical effects, such as the properties of exceptional points in non-Hermitian systems. We have managed not only to extract the real and imaginary parts of the eigenenergies, which determine the topology of the exceptional point, but also to study the eigenstates and their variation with parameters. The main property of exceptional points is the divergence of the characteristic derivatives in their vicinity. This divergence is responsible for enhanced sensing properties of these points. While it is very well known that the derivative of the real part of the energy diverges as $q^{-1/2}$, the hyperbolic q^{-1} divergence of the eigenstates measured by the quantum metric is much less known. Yet, it determines the overlap integrals and, therefore, the possibilities to excite and to measure the states in the vicinity of exceptional points and, ultimately, to benefit from the enhanced sensing.

The possibilities of extraction of the eigenstates and their metric are determined by the experimental resolution in the reciprocal space. In our case, we had to use the axis with the smallest experimental step in order to get sufficiently close to the exceptional point and to be able to evidence the particular power law of the divergence. The observation of this power law on a larger scale would require smaller steps and higher stability of the experimental platform, in order to avoid the broadening in the k space. Disorder-induced mixing of the wave vectors also restrains the possibilities of approaching the exceptional point. The same considerations apply to enhanced sensing: Enhancement applies not only to the useful signal, but also to the noise [38], which, therefore, must be reduced as much as possible.

In conclusion, we have studied exceptional points in an organic microcavity. We have extracted the Stokes vectors of the eigenstates in the vicinity of the exceptional point and then calculated the quantum metric tensor. Our measurements confirm that the quantum metric of a second-order exceptional point exhibits a hyperbolic divergence. This is expected to affect the dynamics of wave packet (the trajectories of optical beams) at exceptional points.

This work was supported by the National Key R&D Program of China (Grants No. 2017YFA0204503 and No. 2018YFA0704805), the National Natural Science Foundation of China (12074303, 11804267, 22090022, 21673144, 21790364, 21873065, and 21833005), the Key Scientific and Technological Innovation Team of Shaanxi Province (2021TD-56), the Beijing Natural Science Foundation of China (21JB0005), the High-level Teachers in Beijing Municipal Universities in the Period of 13th Five-year Plan (IDHT20180517 and CIT&TCD20180331), Beijing Talents Project (2019A23), the Open Fund of the State Key Laboratory of Integrated Optoelectronics (IOSKL2019KF01), Capacity Building for Sci-Tech Innovation-Fundamental Scientific Research Funds, and Beijing Advanced Innovation Center for Imaging Theory and Technology. We acknowledge the support of the projects EU "QUANTOPOL" (846353) and "Quantum Fluids of Light" (ANR-16-CE30-0021) of the ANR Labex Ganex (ANR-11-LABX-0014) and of the ANR program "Investissements d'Avenir" through the IDEX-ISITE initiative 16-IDEX-0001 (CAP 20-25). The authors thank Dr. HW Yin from Ideaoptics Inc. for the support on the angle-resolved spectroscopy measurements. Q. L., C. L., and J. R. contributed equally to this work.

*liaoqing@cnu.edu.cn
†felix831204@xjtu.edu.cn
‡dmitry.solnyshkov@uca.fr

[1] J. Provost and G. Vallee, Riemannian structure on manifolds of quantum states, Commun. Math. Phys. **76**, 289 (1980).
[2] M. Berry, The quantum phase, and five years after, in *Geometric Phases in Physics* (World Scientific, Singapore, 1989), p. 7.
[3] M. V. Berry and P. Shukla, Quantum metric statistics for random-matrix families, J. Phys. A **53**, 275202 (2020).
[4] M. Yu, P. Yang, M. Gong, Q. Cao, Q. Lu, H. Liu, S. Zhang, M. B. Plenio, F. Jelezko, T. Ozawa, N. Goldman, and J. Cai, Experimental measurement of the quantum geometric tensor using coupled qubits in diamond, Natl. Sci. Rev. **7**, 254 (2020).
[5] A. Gianfrate, O. Bleu, L. Dominici, V. Ardizzone, M. De Giorgi, D. Ballarini, G. Lerario, K. West, L. Pfeiffer, D. Solnyshkov, D. Sanvitto, and G. Malpuech, Measurement of the quantum geometric tensor and of the anomalous Hall drift, Nature (London) **578**, 381 (2020).
[6] Y. Gao, S. A. Yang, and Q. Niu, Field Induced Positional Shift of Bloch Electrons and Its Dynamical Implications, Phys. Rev. Lett. **112**, 166601 (2014).
[7] O. Bleu, G. Malpuech, Y. Gao, and D. D. Solnyshkov, Effective Theory of Nonadiabatic Quantum Evolution Based on the Quantum Geometric Tensor, Phys. Rev. Lett. **121**, 020401 (2018).
[8] T. Holder, D. Kaplan, and B. Yan, Consequences of time-reversal-symmetry breaking in the light-matter interaction: Berry curvature, quantum metric, and diabatic motion, Phys. Rev. Research **2**, 033100 (2020).
[9] S. Peotta and P. Törmä, Superfluidity in topologically nontrivial flat bands, Nat. Commun. **6**, 8944 (2015).
[10] L. Liang, S. Peotta, A. Harju, and P. Törmä, Wave-packet dynamics of Bogoliubov quasiparticles: Quantum metric effects, Phys. Rev. B **96**, 064511 (2017).
[11] F. Piéchon, A. Raoux, J.-N. Fuchs, and G. Montambaux, Geometric orbital susceptibility: Quantum metric without Berry curvature, Phys. Rev. B **94**, 134423 (2016).
[12] U. Marzolino and D. Braun, Precision measurements of temperature and chemical potential of quantum gases, Phys. Rev. A **88**, 063609 (2013).
[13] D. Braun, G. Adesso, F. Benatti, R. Floreanini, U. Marzolino, M. W. Mitchell, and S. Pirandola, Quantum-enhanced measurements without entanglement, Rev. Mod. Phys. **90**, 035006 (2018).

[14] A. Srivastava and A. Imamoglu, Signatures of Bloch-Band Geometry on Excitons: Nonhydrogenic Spectra in Transition-Metal Dichalcogenides, Phys. Rev. Lett. **115**, 166802 (2015).
[15] N. Moiseyev, *Non-Hermitian Quantum Mechanics* (Cambridge University Press, Cambridge, England, 2011).
[16] V. V. Konotop, J. Yang, and D. A. Zezyulin, Nonlinear waves in $\mathcal{PT}$-symmetric systems, Rev. Mod. Phys. **88**, 035002 (2016).
[17] R. El-Ganainy, K. G. Makris, M. Khajavikhan, Z. H. Musslimani, S. Rotter, and D. N. Christodoulides, Non-Hermitian physics and PT symmetry, Nat. Phys. **14**, 11 (2018).
[18] Ş. Özdemir, S. Rotter, F. Nori, and L. Yang, Parity–time symmetry and exceptional points in photonics, Nat. Mater. **18**, 783 (2019).
[19] B. Peng, Ş. K. Özdemir, F. Lei, F. Monifi, M. Gianfreda, G. L. Long, S. Fan, F. Nori, C. M. Bender, and L. Yang, Parity–time-symmetric whispering-gallery microcavities, Nat. Phys. **10**, 394 (2014).
[20] T. J. Milburn, J. Doppler, C. A. Holmes, S. Portolan, S. Rotter, and P. Rabl, General description of quasiadiabatic dynamical phenomena near exceptional points, Phys. Rev. A **92**, 052124 (2015).
[21] J. Doppler, A. A. Mailybaev, J. Böhm, U. Kuhl, A. Girschik, F. Libisch, T. J. Milburn, P. Rabl, N. Moiseyev, and S. Rotter, Dynamically encircling an exceptional point for asymmetric mode switching, Nature (London) **537**, 76 (2016).
[22] W. Chen, Ş. K. Özdemir, G. Zhao, J. Wiersig, and L. Yang, Exceptional points enhance sensing in an optical microcavity, Nature (London) **548**, 192 (2017).
[23] D. Leykam, K. Y. Bliokh, C. Huang, Y. D. Chong, and F. Nori, Edge Modes, Degeneracies, and Topological Numbers in Non-Hermitian Systems, Phys. Rev. Lett. **118**, 040401 (2017).
[24] H. Shen, B. Zhen, and L. Fu, Topological Band Theory for Non-Hermitian Hamiltonians, Phys. Rev. Lett. **120**, 146402 (2018).
[25] M. Berry and R. Uzdin, Slow non-Hermitian cycling: Exact solutions and the stokes phenomenon, J. Phys. A **44**, 435303 (2011).
[26] M. Berry, Optical polarization evolution near a non-Hermitian degeneracy, J. Opt. **13**, 115701 (2011).
[27] D. C. Brody and E. M. Graefe, Information geometry of complex Hamiltonians and exceptional points, Entropy **15**, 3361 (2013).
[28] D. D. Solnyshkov, C. Leblanc, L. Bessonart, A. Nalitov, J. Ren, Q. Liao, F. Li, and G. Malpuech, Quantum metric and wave packets at exceptional points in non-Hermitian systems, Phys. Rev. B **103**, 125302 (2021).
[29] M. V. Berry and M. R. Dennis, The optical singularities of birefringent dichroic chiral crystals, Proc. R. Soc. A **459**, 1261 (2003).
[30] W. Voigt, On the behaviour of pleochroitic crystals along directions in the neighbourhood of an optic axis, Philos. Mag. Ser. 5 **4**, 90 (1902).
[31] S. Richter, H.-G. Zirnstein, J. Zúñiga-Pérez, E. Krüger, C. Deparis, L. Trefflich, C. Sturm, B. Rosenow, M. Grundmann, and R. Schmidt-Grund, Voigt Exceptional Points in an Anisotropic ZnO-Based Planar Microcavity: Square-Root Topology, Polarization Vortices, and Circularity, Phys. Rev. Lett. **123**, 227401 (2019).
[32] A. Kavokin, J. J. Baumberg, G. Malpuech, and F. P. Laussy, *Microcavities* (Oxford University Press, New York, 2011).
[33] J. Ren, Q. Liao, H. Huang, Y. Li, T. Gao, X. Ma, S. Schumacher, J. Yao, S. Bai, and H. Fu, Efficient bosonic condensation of exciton polaritons in an h-aggregate organic single-crystal microcavity, Nano Lett. **20**, 7550 (2020).
[34] See Supplemental Material at http://link.aps.org/supplemental/10.1103/PhysRevLett.127.107402 for more details on the experiments and on the theoretical description of the quantum metric.
[35] K. Rechcińska, M. Król, R. Mazur, P. Morawiak, R. Mirek, K. Łempicka, W. Bardyszewski, M. Matuszewski, P. Kula, W. Piecek, P. G. Lagoudakis, B. Pietka, and J. Szczytko, Engineering spin-orbit synthetic Hamiltonians in liquid-crystal optical cavities, Science **366**, 727 (2019).
[36] J. Ren, Q. Liao, F. Li, Y. Li, O. Bleu, G. Malpuech, J. Yao, H. Fu, and D. Solnyshkov, Nontrivial band geometry in an optically active system, Nat. Commun. **12**, 689 (2021).
[37] C. M. Bender and S. Boettcher, Real Spectra in Non-Hermitian Hamiltonians Having $\mathcal{PT}$ Symmetry, Phys. Rev. Lett. **80**, 5243 (1998).
[38] J.-H. Park, A. Ndao, W. Cai, L. Hsu, A. Kodigala, T. Lepetit, Y.-H. Lo, and B. Kanté, Symmetry-breaking-induced plasmonic exceptional points and nanoscale sensing, Nat. Phys. **16**, 462 (2020).